# Polarization of $^{12}B$ produced in $^{14}N$-induced reactions

K. H. Tanaka,* Y. Nojiri, T. Minamisono, K. Asahi,† and N. Takahashi‡
*Laboratory of Nuclear Studies and Department of Physics, Faculty of Science, Osaka University, Toyonaka, Osaka, 560 Japan*

(Received 28 October 1985; revised manuscript received 14 April 1986)

Nuclear spin polarization of projectile-like fragments $^{12}B$ produced in ($^{14}N$,$^{12}B$) reactions at around the classical grazing angle was measured as a function of reaction $Q$ value at incident energies of 120 and 200 MeV. Large positive $^{12}B$ polarization was observed in the region of small kinetic energy loss for heavy target nuclei ranging from $^{232}Th$ to $^{nat}Fe$, and it was interpreted in terms of direct two-proton transfer. For the target nucleus $^{27}Al$, however, large negative polarization was observed in the region of small kinetic energy loss. It was found that the $^{45}Sc$ target nucleus was situated at a crossover point for the sign of the polarization. This fact is explained by assuming coexistence of direct and frictional processes. It is found that the contribution of the frictional process tends to exceed that of the direct process with a decrease of target mass number in the region of small energy loss. In the region of large kinetic energy loss, the dominant mechanism is due to the frictional process. A friction constant of $(2.4\pm0.5)\times10^{-22}$ MeV s/fm$^2$ is deduced from the present experimental data. This value agrees in order of magnitude with that obtained from the recent study on the reaction Xe + Bi.

## I. INTRODUCTION

A system of two colliding nuclei in heavy-ion reactions usually sustains a large amount of orbital angular momentum of relative motion. As demonstrated by experiments on multiplicity and anisotropy of nuclear radiations emitted from reaction products, a part of orbital angular momentum is transformed into the intrinsic spins of product nuclei. Our main concern is, then, to clarify this transformation process and thus to probe the heavy-ion reaction mechanisms through polarization phenomena. Polarization of reaction products and the amount of the transferred angular momentum allow us an important insight into the transfer process and the reaction mechanism. As an example, let us consider a macroscopic friction model for heavy-ion collisions, where the angular momentum transfer is caused by the tangential component of the frictional force. Polarization directs itself along the direction of orbital angular momentum relative to the reaction trajectory.[1] It is possible to test the validity of this model by observing polarization phenomena.

It is, however, generally difficult to determine the sign of polarization solely from measurements of multiplicity or anisotropy, since these quantities carry information only on the spin value and alignment of the nuclear state. It is thus indispensable to find other methods which could be applied directly to determination of polarization. For this purpose two methods have been developed so far. One is to measure asymmetric $\beta$ decay[2,3] and the other is to measure circular polarization of $\gamma$ rays emitted from nuclear excited levels.[4,5] In our previous work,[2,3] $^{12}B$ polarization was measured as a function of reaction $Q$ value for $^{100}Mo(^{14}N,^{12}B)$ by the former method. Except for the region of small kinetic energy loss, the experimental results agreed qualitatively with the prediction of the friction model in a wide range of kinetic energy loss ($Q$ value) and thus clarified an evidence for the orbiting process in heavy-ion reactions. Polarization observed in the region of small energy loss disclosed for the first time the existence of direct two-proton transfer from the projectile to the target nuclei.[2,6] These results show that the polarization measurements are indeed powerful in probing heavy-ion reaction mechanisms.

The present experiment aims at a quantitative understanding of heavy-ion reaction mechanism by observing polarization as a function of reaction $Q$ value, target mass number $A_2$, reaction angle $\theta_L$, and incident energy $E_i$. Polarization of ejectiles was measured with various target nuclei at two bombarding energies as a function of reaction $Q$ value. A systematic behavior of polarization was observed, and an averaged friction constant $(2.4\pm0.5)\times10^{-22}$ MeV s/fm$^2$ is extracted from crossover of sign of polarization. Also disclosed was a phenomenon that the frictional process prevails even in the region of small energy loss and competes with the direct transfer process.

The bases and details of the experimental method are given in Sec. II and the experimental results are presented in Sec. III. The discussion of the results is given in Sec. IV in connection with the reaction mechanism.

## II. EXPERIMENTAL METHODS

The energy spectrum of projectile-like products of heavy-ion reactions at the incident energy of approximately 10 MeV/nucleon is widely distributed from the maximum energy corresponding to $Q_{gg}$ (Ref. 7) down to the Coulomb energy $V_C$, where the kinetic energy of reaction products corresponds to the Coulomb repulsive energy of two spherical nuclei in the final state of collision. Energy spectra of $^{12}B_{g.s.}$ ($I^\pi=1^+$, $T_{1/2}=20.3$ ms, and $E_{\beta max}=13.4$ MeV) in $^{14}N$-induced reactions are not the excep-

 

tion. In the measurements of polarization of $^{12}$B with broad kinetic energy distribution, two methods have been adopted here:[8] range analysis to select a kinetic-energy window of $^{12}$B and measurement of $\beta$-decay asymmetry by use of NMR to determine $^{12}$B polarization. A pulsed beam was used to reduce background for detection of $\beta$ rays. $^{12}$B nuclei were uniquely identified from the NMR frequency, the high $\beta$-ray maximum energy, and the lifetime.

### A. Experimental setup

The experiments were carried out at the Research Center for Nuclear Physics (RCNP), Osaka University. A $^{14}$N beam of approximately 500 pnA accelerated by the 230 cm azimuthally varying field (AVF) cyclotron was focused onto the target in a spot of approximately 3 mm in diameter. Energies of the beam were 210 MeV for 5+ ions and 130 MeV for 4+ ions. The targets were metallic foils approximately 10 mg/cm$^2$ thick, in which the energy loss of the incident $^{14}$N ion was about 20 MeV. The mean incident energy $E_i$ was defined as an energy at the middle of the target. The schematic illustration of the experimental setup is shown in Fig. 1(a). The primary beam passing through the target was collected in a beam dump placed inside the target chamber. The reaction products $^{12}$B were collimated and implanted into a Pt stopper, after passing through an Al energy absorber. The stopper chamber was movable around the target between 6° and 60° relative to the incident beam. Angular acceptance was ±4° with the corresponding solid angle of 30 msr. To reduce the backward scattering of $\beta$ rays from the chamber wall, the stopper chamber was made of nylon. For the same reason, use of heavy elements was avoided in the vicinity of the stopper area. A pair of radio frequency (rf) coils for NMR was mounted outside the stopper chamber [see Fig. 1(b)] and a pair of iron-free electric coils was used to produce the static magnetic field $H_0$ parallel to the reaction normal.

Two sets of plastic-scintillation-counter telescopes were used to detect $\beta$ rays. They were placed above and below the stopper with their axes parallel to the reaction normal. The solid angle subtended by the telescope was 270 msr. Each telescope consisted of two $\Delta E$ counters ($A$, 12 mm in diameter and 1 mm thick; $B$, 46 mm in diameter and 2 mm thick) and one energy counter ($E$, 60 mm in diameter and 70 mm thick). An additional conical anticoincidence counter ($C$) was placed between $A$ and $B$ as shown in Fig. 1(a) to reject the scattered $\beta$ rays. Anticoincidence signals were also obtained from $A$ and $C$ counters of the opposite telescope. The definition of a true $\beta$-ray event was

$$(A\times B\times\bar{C}\times E)\times(\bar{A}\times\bar{C})_{\text{opposite}}$$

with a resolving time of 20 ns. The energy threshold level for $\beta$-ray detection was set at 3 MeV. The accidental coincidence rate was thus reduced to less than 1%.

A schematic time chart of the measurement is shown in Fig. 2, including the irradiation, spin control, and $\beta$-ray counting. The beam repetition period was 64 ms. During the first 29 ms the target was bombarded by $^{14}$N ions. The following 35 ms were without beam and were used for polarization control and the $\beta$-ray counting. Polarization was inverted by means of adiabatic-fast-passage (AFP) NMR during 2.5 ms following the end of the every other beam cycle. The same NMR was applied for 2.5 ms at the end of the relevant off-beam time to restore the polarization direction. The inversion of polarization was made, thus, in every other counting period. In the next cycle, the rf field was applied at off-resonance frequency and $^{12}$B polarization was not inverted. These two cycles

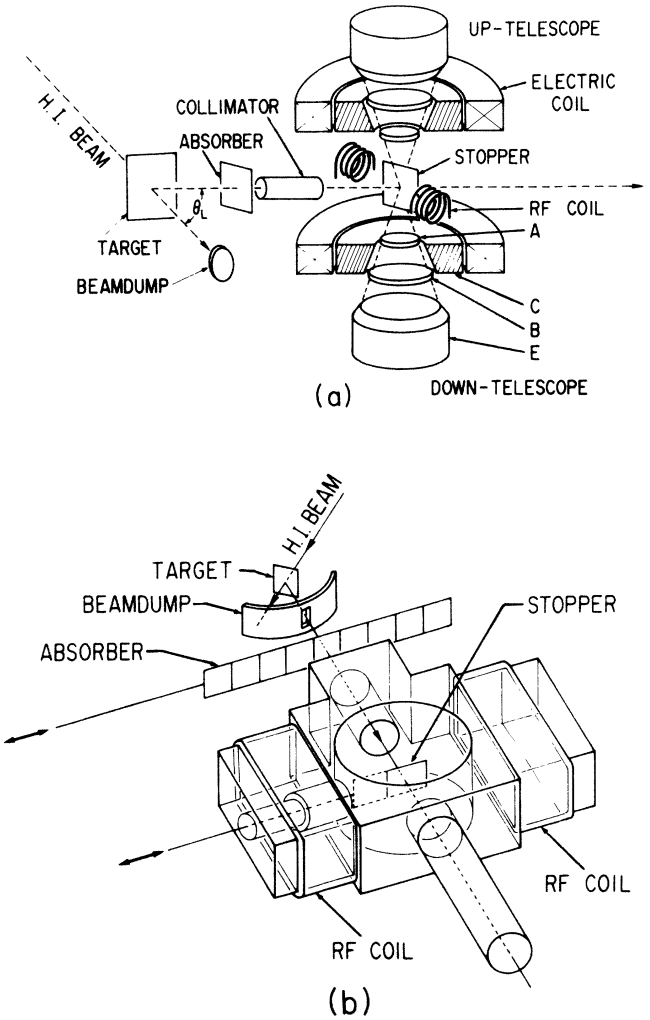


FIG. 1. (a) Schematic illustration of the measuring system. The reaction product $^{12}$B was collected at a reaction angle $\theta_L$ and was implanted into a stopper. An energy absorber was placed between the target and the stopper. A pair of air-core electric coils produced a static magnetic field perpendicular to the reaction plane around the stopper. Polarization of reaction product was preserved in the stopper long enough to be controlled by NMR induced by a set of rf coils placed around the stopper, and to detect asymmetric $\beta$ decay from the polarized $^{12}$B by a pair of counter telescopes placed above and below the reaction plane. (b) Detailed illustration of the stopper chamber. The stopper chamber was made of nylon and a pair of rf coils for NMR was mounted outside the chamber to reduce the scattering of $\beta$ rays.

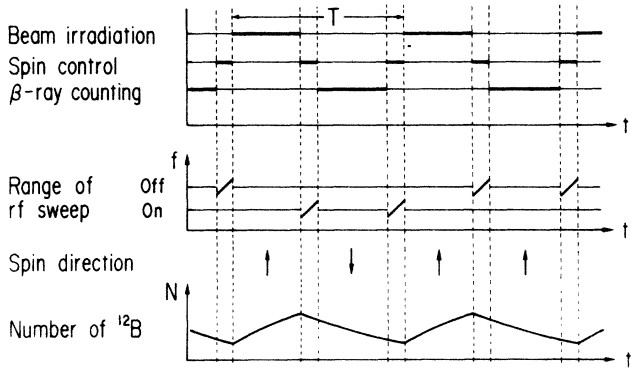


FIG. 2. Time sequence of the polarization measurement, i.e., the beam irradiation, spin control, and $\beta$-ray counting. The basic cycle $T$ was 64 ms.

were alternately repeated. Thus, polarization was determined to be free from geometrical asymmetries of the measuring system. The time sequence of the experiment was supervised by a microprocessor. The pulsing of $^{14}$N beams was realized by reducing the acceleration voltage of the cyclotron to 70% during the off-beam period.

### B. Implantation of $^{12}$B and preservation of polarization

The kinetic-energy window for $^{12}$B implanted into the stopper was specified by use of a range-energy method.[9] The energy window for $^{12}$B implanted in the stopper was determined by the thicknesses of the aluminum absorber and of the platinum stopper. $^{12}$B nuclei with kinetic energy below the energy window were stopped in the absorber and those above the energy window passed through the stopper. The ambiguity in the estimation of $^{12}$B kinetic energy came mainly from range straggling and was less than 5%.

The polarization of $^{12}$B with kinetic energy above 11 MeV was maintained during its flight, since the ions leaving the target were stripped of all electrons and no hyperfine interaction in the ions was effective. The spin of the $^{12}$B nucleus was not flipped by the electromagnetic interactions during its penetration through the absorber and the stopper since the access time of collision with an atom was too short for the spin of $^{12}$B to rotate appreciably. The $^{12}$B nuclei, however, with energies less than 11 MeV, might be under the influence of strong atomic hyperfine fields during their flight in vacuum since few-electron configurations could be dominant.

To subtract the possible depolarization effects, an additional measurement was carried out with a stopper of a thickness corresponding to the range of 11 MeV $^{12}$B. After a pair of measurements the $\beta$-ray counts obtained with the thin stopper were subtracted properly from those with the thick one. Background $\beta$ rays emitted from sources other than the stopper were—in this procedure—subtracted at the same time.

The technique of polarization control has already been established.[10] For example, it has been shown that the NMR line for $^{12}$B is as sharp as the dipolar broadening due to the nuclear moments of the surrounding nuclei at room temperature. This fact means that $^{12}$B at rest in a Pt stopper after the implantation is free from the effects of radiation damage produced by the traveling $^{12}$B ion itself before it stopped and the elastically scattered incident beam. The spin-lattice relaxation time for $^{12}$B in Pt is 10 times longer than the lifetime of $^{12}$B at room temperature.[11,12]

### C. Determination of polarization

The angular distribution of $\beta$ rays is given as[13]

$$W(\phi)=1+(v/c)PA\cos\phi\ , \tag{2.1}$$

where $v/c$ is the ratio of speed of $\beta$ ray to the light velocity and is close to 1 for $\beta$ rays with energy higher than the threshold energy. The asymmetry is due to parity nonconservation in the weak interaction. Here, $P$ is nuclear polarization, $A$ is the asymmetry parameter, and $\phi$ is the polar angle of $\beta$-ray momentum relative to the polarization axis. In the present experiment $A$ is close to $-1$, since the major decay branch is an allowed Gamow-Teller—type, i.e., $1^+$ to $0^+$, state of $^{12}$C. To measure $P$ free from geometrical asymmetries in the $\beta$-ray detection system, the $\beta$-ray distributions with and without polarization inversion were compared. The ratio $R$ between the counting rates in $\beta$-ray detectors placed above ($\phi=0$) and below ($\phi=\pi$) the reaction plane is

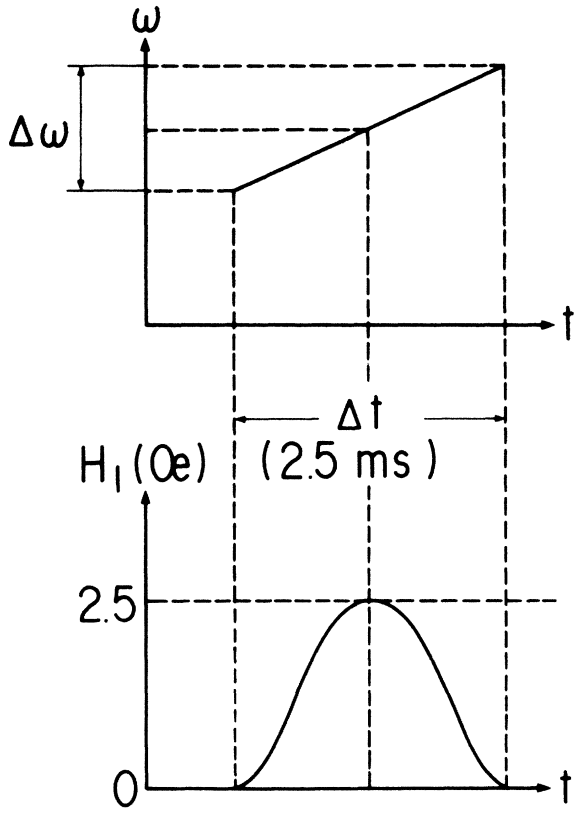


FIG. 3. Sinusoidal modulation of the amplitude and the frequency of $H_1$ as a function of time.

$$R=\{[W(0)_{\rm off}/W(\pi)_{\rm off}]/[W(0)_{\rm on}/W(\pi)_{\rm on}]\}^{1/2} . \quad (2.2)$$

Here the subscripts on and off refer to the spin inversion on and off, respectively. Thus $P$ is given as

$$P=(1-R)/(1+R) . \quad (2.3)$$

Here the sign of polarization parallel to the reaction normal

$$\mathbf{n}=(\mathbf{k}_i\times\mathbf{k}_f)/|\mathbf{k}_i\times\mathbf{k}_f|$$

is taken as positive, where $\mathbf{k}_i$ and $\mathbf{k}_f$ are incoming and outgoing wave vectors, respectively.

### D. Control of spin polarization

For the polarization inversion, an adiabatic-fast-passage (AFP) method in the NMR technique was used. Immediately after the end of the beam irradiation, a rf magnetic field $H_1\cos(\omega t)$ was applied by a pair of rf coils perpendicularly to the static magnetic field ($H_0=221$ Oe) and in parallel to the surfaces of the stopper [see Fig. 1(a)] for 2.5 ms. The rf field was swept from 159 to 179 kHz across the resonance frequency $\gamma H_0/2\pi=169$ kHz, where $\gamma$ is the gyromagnetic ratio of $^{12}$B $\gamma=2\pi\times765$ Hz/Oe.[12] The requirements on the rf intensity for AFP is

$$\Delta\omega/\Delta t \ll (\gamma H_1)^2 . \quad (2.4)$$

Here, $\Delta\omega/2\pi$ is the range of frequency modulation and $\Delta t$ is a period of rf sweep. In the present experiment, an $H_1$ of about 2.5 Oe was employed; therefore, the strength of $H_1$ was large enough to fulfill the condition (2.4) and, in addition, $H_1$ was stronger than the intrinsic broadening in the stopper material, which amounted to less than 1 Oe in Pt. The amplitude $H_1$ was modulated sinusoidally as a function of time (see Fig. 3) to achieve the greatest degree of polarization inversion.[10]

### E. The degree of spin control achieved

The strengths of the external field $H_0$, of the frequency range, and of the rf field for AFP were optimized with the present experimental setup prior to the main run by use of polarized $^{12}$B produced in the $^{11}$B(d,p)$^{12}$B reaction[12] using the Van de Graaff accelerator at the Laboratory of Nuclear Studies, Osaka University.

Previous work[12] has shown that depolarization effects on $^{12}$B in Pt due to radiation damage and dipolar interaction can be decoupled by applying an external magnetic field of $H_0>150$ Oe. Thus, a practical value of $H_0$ was chosen to be 221 Oe. The rf modulation of 20 kHz safely covered the NMR linewidth, which is mainly due to the field inhomogeneity of 2%. The degree of achievement of the spin inversion was better than 95%. The spin-lattice-relaxation time for $^{12}$B in Pt was 300 ms at room temperature, consistent with the previous results.[12] Therefore it can be concluded that the polarization measured in the main run is approximately 90% of that produced in the reaction. Correction for this depolarization effect is discussed at the end of the following section.

## III. EXPERIMENTAL RESULTS

Polarization of $^{12}$B from ($^{14}$N,$^{12}$B) reactions was measured for various species of target nuclei at approximately 120 MeV and at 200 MeV. The experimental conditions are summarized in Table I. Dependence of polarization on $Q$ value showed similar behavior for target nuclei $^{232}$Th, $^{100}$Mo, $^{nat}$Cu, and $^{nat}$Fe similar to what was observed for the reaction $^{100}$Mo($^{14}$N,$^{12}$B) at 90 MeV (note that the definition of the sign of $P$ in this paper is different from that in Ref. 2). New features of the polarization were found in the present systematic study: The kinetic energy for the point of crossover for the sign of polarization was dependent on the target mass number and

TABLE I. Experimental conditions for the reactions studied and $Q$ values for the FZC and SZC.

| Target | $E_i$ (MeV) | $\theta_L$ (deg) | $-Q$(FZC) (MeV) | $-Q$(SZC) (MeV) |
|---|---|---|---|---|
| $^{27}$Al | 115 | 6 | not seen | 25±5 |
| | 115 | 10 | not seen | 27±5 |
| | 120 | 20 | not seen | 25±5 |
| | 200 | 20 | not seen | 38±6 |
| $^{45}$Sc | 114 | 13 | not seen | 24±5 |
| | 114 | 20 | not seen | 34±5 |
| $^{nat}$Fe | 116 | 15 | not seen | 35±5 |
| | 112 | 25 | 35±5 | 35±5 |
| $^{nat}$Cu | 120 | 20 | 35±5 | 35±5 |
| $^{100}$Mo | 122 | 13 | 42±6 | 53±6 |
| | 122 | 20 | 35±5 | 51±6 |
| | 120 | 25 | 31±5 | 49±7 |
| | 120 | 35 | 25±7 | 37±7 |
| | 200 | 20 | 37±7 | 73±8 |
| $^{232}$Th | 129 | 30 | 38±5 | 90±7 |
| | 200 | 30 | 45±11 | not seen |

the reaction angle. Also found was large negative polarization in the region of small kinetic energy loss for the reactions with light target nuclei.[14] For $^{27}$Al, for instance, polarization in the region of small energy loss showed a drastic contrast to the data for target nuclei heavier than $^{nat}$Fe.

### A. Dependence on target mass

Polarization and yield of $^{12}$B from ($^{14}$N,$^{12}$B) at 120 MeV are shown in Figs. 4(a)—4(f) as functions of kinetic energy of $^{12}$B near the grazing angle for target nuclei $^{27}$Al, $^{45}$Sc, $^{nat}$Fe, $^{nat}$Cu, $^{100}$Mo, and $^{232}$Th. The vertical bars show the statistical uncertainties, whereas the horizontal bars indicate the kinetic energy ($Q$-value) windows chosen.

Large positive polarization was clearly observed in the region of small energy loss for heavy target nuclei $^{nat}$Fe, $^{nat}$Cu, $^{100}$Mo, and $^{232}$Th, and polarization became negative or vanished with increasing energy loss. The reaction $Q$ value for the kinetic energy where polarization crosses

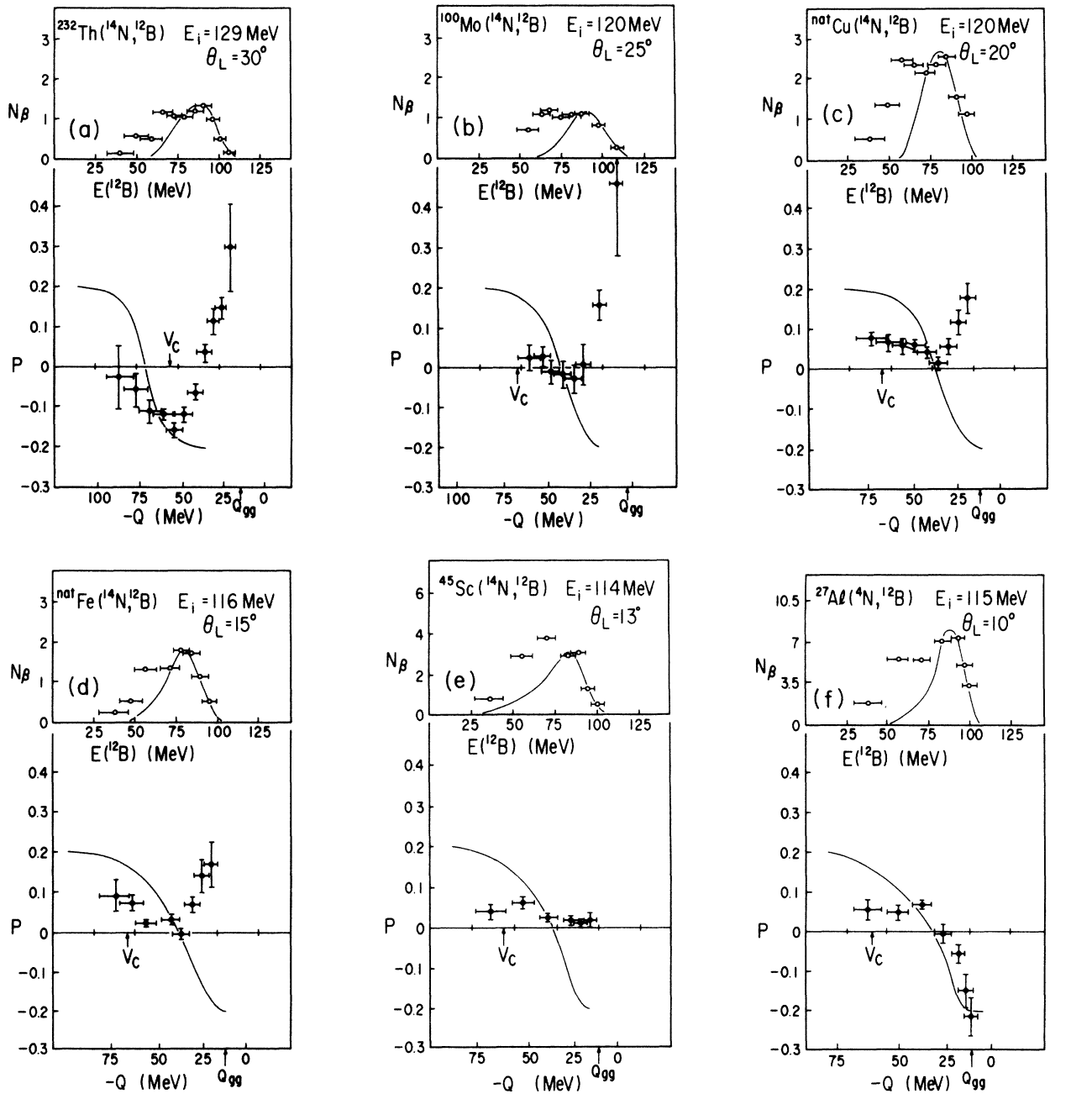


FIG. 4. (a)—(f) Experimental results of $^{12}$B polarization and energy spectrum obtained near the grazing angle for various targets. The vertical bars are the statistical uncertainties and the horizontal bars show the width of kinetic energy ($Q$-value) window deduced from the range-energy relation. Results of calculation by use of quasilinear response theory (QLRT) are also shown by solid curves. The theoretical values of the polarization are multiplied by a factor 0.2.

zero was almost constant for each target. Polarization showed another zero crossing and became positive again with further increasing kinetic energy loss. On the other hand, the reaction $Q$ value for the latter zero crossing was shifted to larger energy loss with increasing target mass number $A_2$. The zero crossing in the region of small kinetic energy loss is referred to as the first zero crossing (FZC) and that in the region of large kinetic energy loss as the second zero crossing (SZC). These are shown schematically in Fig. 5. The dependence of the polarization on the target mass number $A_2$ can be summarized as follows: (1) The FZC was at an energy loss almost independent of $A_2$ for targets heavier than $^{nat}$Fe when the reaction angle was near the grazing angle [see Fig. 6(a)]. (2) The SZC always appeared for all the target nuclei and shifted towards large energy loss with increasing $A_2$ [see Fig. 6(b)]. As stated before, another trend of the polarization was observed in the region of small energy loss for light target nuclei, e.g., the sign of polarization was negative for target nucleus $^{27}$Al and was nearly equal to zero for target nucleus $^{45}$Sc. Namely, (3) the FZC disappeared for light target nuclei such as $^{27}$Al and only the SZC was observed, as displayed in Fig. 7.

Even at a higher incident energy of 200 MeV, the behavior of $^{12}$B polarization was essentially the same as measured at 120 MeV. Spectra and polarization from ($^{14}$N,$^{12}$B) reactions on $^{232}$Th, $^{100}$Mo, and $^{27}$Al are shown in Fig. 8. Here, $^{12}$B polarization was measured at the grazing angle or at an angle slightly more backward. The polarization data at 200 MeV are summarized in Fig. 9.

### B. Dependence on reaction angle

Polarizations at various reaction angles are shown in Fig. 10 and the data are assembled in Fig. 11.

Two features of polarization was observed as a function of reaction angle. One was the shift of the FZC as a function of reaction angle observed for target nuclei heavier than $^{nat}$Fe. The FZC moved to smaller energy loss with increasing reaction angle. It should be noted that the FZC appeared only at backward angles for $^{45}$Sc and did not appear even at backward angles for $^{27}$Al. This is summarized as follows: (4) The FZC shifted towards the region of smaller energy loss with increasing reaction angle for target nuclei for $^{nat}$Fe through $^{232}$Th.

Another feature, (5), was the systematic change of the magnitude of polarization as a function of reaction angle. The polarization of $^{12}$B in the energy region lower than

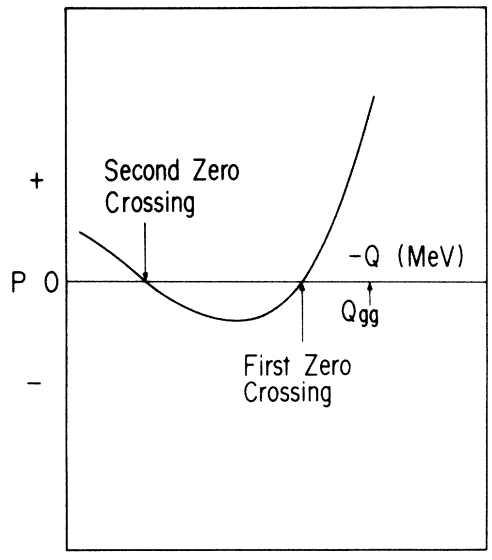


FIG. 5. Illustration of the first zero crossing (FZC) and the second zero crossing (SZC).

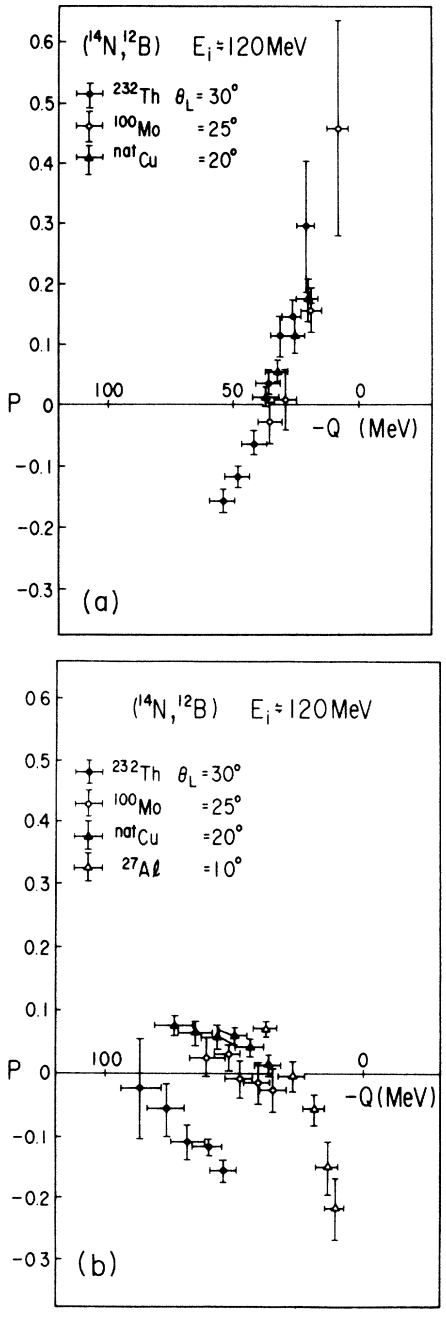


FIG. 6. Superimposed illustration of the experimental polarization for various target nuclei measured near the grazing angle around the (a) FZC and (b) the SZC.

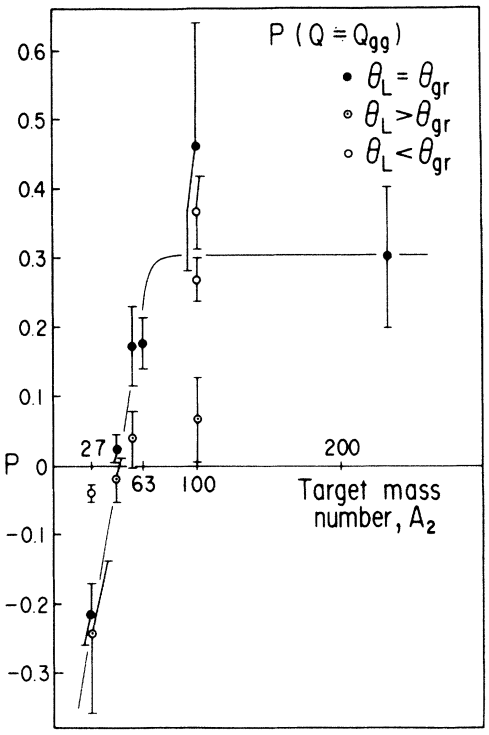


FIG. 7. Polarization at around $Q_{gg}$ plotted against target mass number $A_2$. The crossover from negative and positive polarizations is at about mass 45. The solid line is a guide to the eyes.

the SZC became larger with increasing reaction angle. As a typical example, the maximum value of positive polarization for $^{27}$Al($^{14}$N,$^{12}B$) was about $-20\%$ at $\theta_L=20°$, about $-8\%$ at $\theta_L=10°$, and about $-4\%$ at $\theta_L=6°$. Similar trends were also observed for the reactions on $^{nat}$Fe and $^{45}$Sc.

### C. Possible depolarization effects in the experiment

There are four possible causes of the reduction in magnitude of the polarization of $^{12}B_{g.s.}$ produced in the reaction process before it is measured.

The first two are the production of the $^{12}$B ground state via other processes, i.e., (1) the particle emission $^{13}C \rightarrow p + {}^{12}B$, and (2) the $\gamma$ decay from excited states of $^{12}$B to the ground state. The influence of these branches to the measured $^{12}$B polarization is estimated as follows.

The particle emission does not change, at least, the sign of the initial polarization. From the coincidence experiments between p and $^{12}$B emitted in $^{13}$C decay, Ost *et al.*[15] found that the sequential decay took place mainly in the quasielastic collisions and that the contribution from such decay has been estimated less than 20% of the total yield. This experiment was, however, done at an incident energy of 7.5 MeV/nucleon, where the quasielastic collision was dominant. The main process at the present incident energies is deep inelastic collision and the contribution from such sequential processes is suppressed.

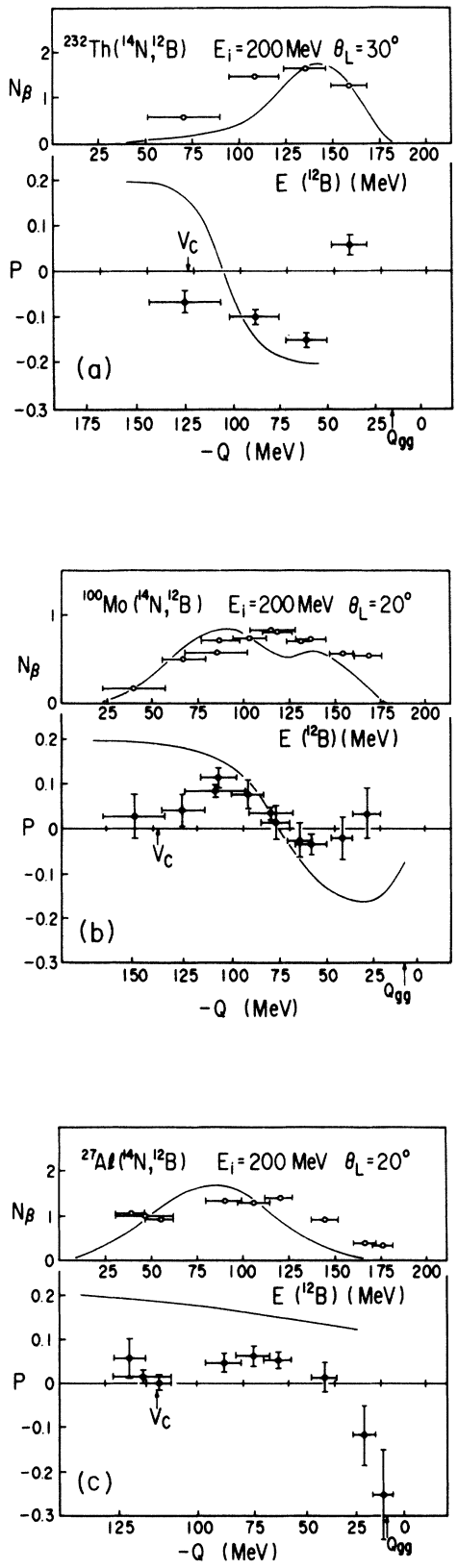


FIG. 8. (a)–(c) Experimental results on $^{12}$B polarization and energy spectrum measured at an incident energy of 200 MeV. The definitions of vertical bars, horizontal bars, and the solid line are the same as in Fig. 4.

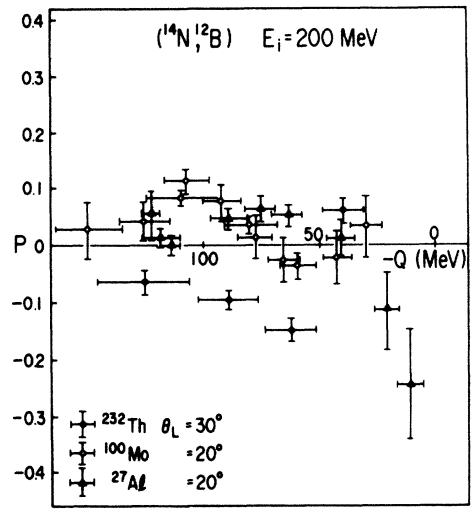


FIG. 9. Superimposed illustration of the experimental polarization measured at an incident energy of 200 MeV for various target nuclei.

Thus, the reduction of polarization due to the particle emission is, at most, 20%.

Only four excited states of $^{12}$B feed the $^{12}B_{g.s.}$ via $\gamma$ decays. The highest excitation energy among those levels is 2.72 MeV slightly less than the neutron separation energy. Thus we assume that these levels are equally populated except for the statistical factors. Since the $\gamma$-decay schemes from these levels have been well established,[16] the depolarization in the $\gamma$-decay processes is estimated as 15% of the initial value from the vector coupling model of angular momenta.

The third thing which affects the magnitude of the initial polarization is the hyperfine interactions of the $^{12}$B nucleus with atomic electrons. Ions during their flight in vacuum before implantation into the stopper are subject to such interactions. Such depolarization is essentially removed by means of the background subtraction using thin and thick stoppers as mentioned in Sec. II B. Depolarization may arise from the spin-lattice relaxation, when ions experience interactions from the normal and radiation-damaged environments in the Pt stopper. As described in Sec. II E, however, the magnetic interaction with an external magnetic field stronger than 150 Oe at 300 K is enough to decouple the nuclear spin from the quadrupole interaction with the radiation damage in Pt. Thus it was possible to preserve the polarization.

The last cause is the contribution of background $\beta$ activities. We identity $^{12}$B nuclei by detecting the high energy $\beta$ rays emitted. The $\beta$-decay time spectrum measured is also used to estimate and to subtract the fraction of the background $\beta$ rays mixed in. However, nuclei such as $^{13}$B and $^{12}$N sustaining similar $\beta$-decay endpoint energies and lifetimes may not be rejected. By use of the empirical $Q_{gg}$ dependence[7] of the isotope production, however, the contribution from $^{13}$B is estimated to be less than 20% of the total $\beta$-ray yield. The production cross sections for $^{12}$N are also estimated to be negligibly small. Thus the reduction of the $^{12}$B polarization due to $^{13}$B is, in all, less than 20% of the initial value.

We therefore conclude that the initial polarization may reach about 2.5 times the experimentally observed values. However, the experimental values of the polarization are not corrected for this attenuation factor, since we evaluate the relative shifts of the FZC and SZC as a good reference to the polarization phenomena, as discussed below. Reaction mechanisms are clarified from the relative value of polarization instead of the absolute value as a function of reaction $Q$ value, as given in the next section.

## IV. DISCUSSION

In the preceding section, five features of the characteristics of the $^{12}$B polarization were summarized. The first two have already been observed in our previous work, i.e., the large positive polarization in the region of small energy loss has disclosed for the first time the importance of the direct two-proton transfer process,[2,6] and the polarization in the region of large energy loss has qualitatively disclosed, within the framework of the classical friction model, the orbiting process in the double-nuclear system (DNS).[17]

The shift of the second zero crossing (SZC) versus target mass number $A_2$ is newly found in the present study and is qualitatively understood by the friction model in the following way. It is assumed that the energy dissipation rate by frictional forces is not drastically changed during the interaction. The projectile-like fragment is to be polarized parallel to the orbital angular momentum and the sign of polarization is inverse to that of the deflection angle.[1] The polarization is proportional to the difference between the partial cross sections at the negative and positive deflection angles. For lighter target nuclei the moment of inertia of the DNS is small, while its rotating velocity is large. The negative-angle deflection for the projectile nucleus can occur in a short interaction time. The fragments emitted into negative angles emerge with small kinetic energy loss, i.e., the SZC thus takes place at the region of small energy loss.

Features (3) and (4) suggest the coexistence of two reaction mechanisms in the region of small energy loss. The frictional process for the positive-angle deflection, which induces the negative polarization, is superimposed on the direct two-proton transfer process which induces the positive polarization. As a result of such mixing, positive polarization characterizing the direct two-proton transfer process either decreases to a negative value or sometimes polarization vanishes completely. It is natural to consider that the contribution of the frictional process becomes larger at backward angles, since the direct process is more peaked toward forward reaction angles than the frictional process. The direct process is pronounced for lighter target nuclei. The ratio between contributions of the two processes is also dependent on the target mass number $A_2$ since the interaction time of the frictional process changes as a function of $A_2$. Since the DNS formed in the frictional process rotates faster in the case of lighter targets, the positive-angle deflection occurs at the region of small energy loss and mixes with the direct process at the for-

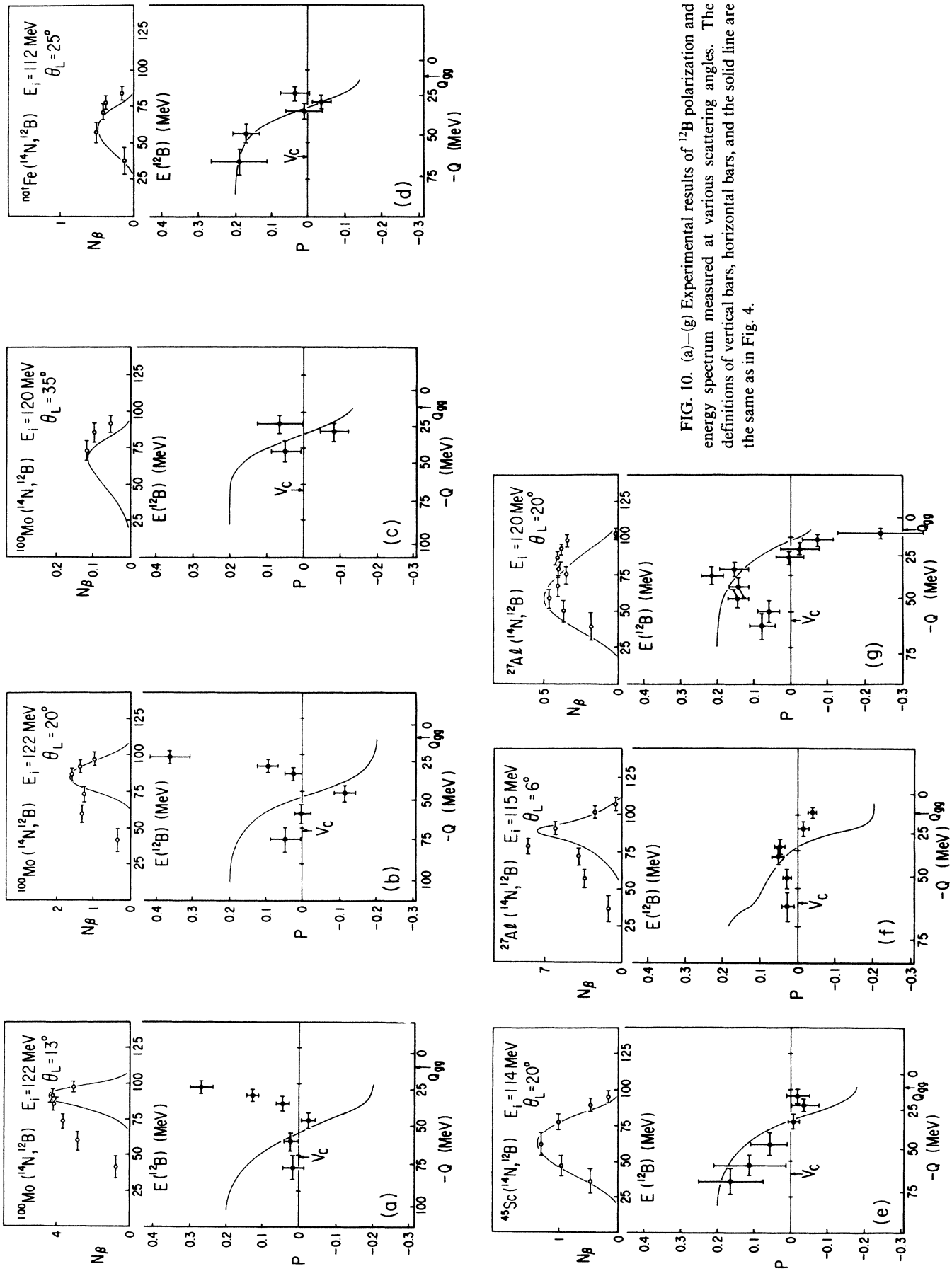


FIG. 10. (a)—(g) Experimental results of $^{12}$B polarization and energy spectrum measured at various scattering angles. The definitions of vertical bars, horizontal bars, and the solid line are the same as in Fig. 4.

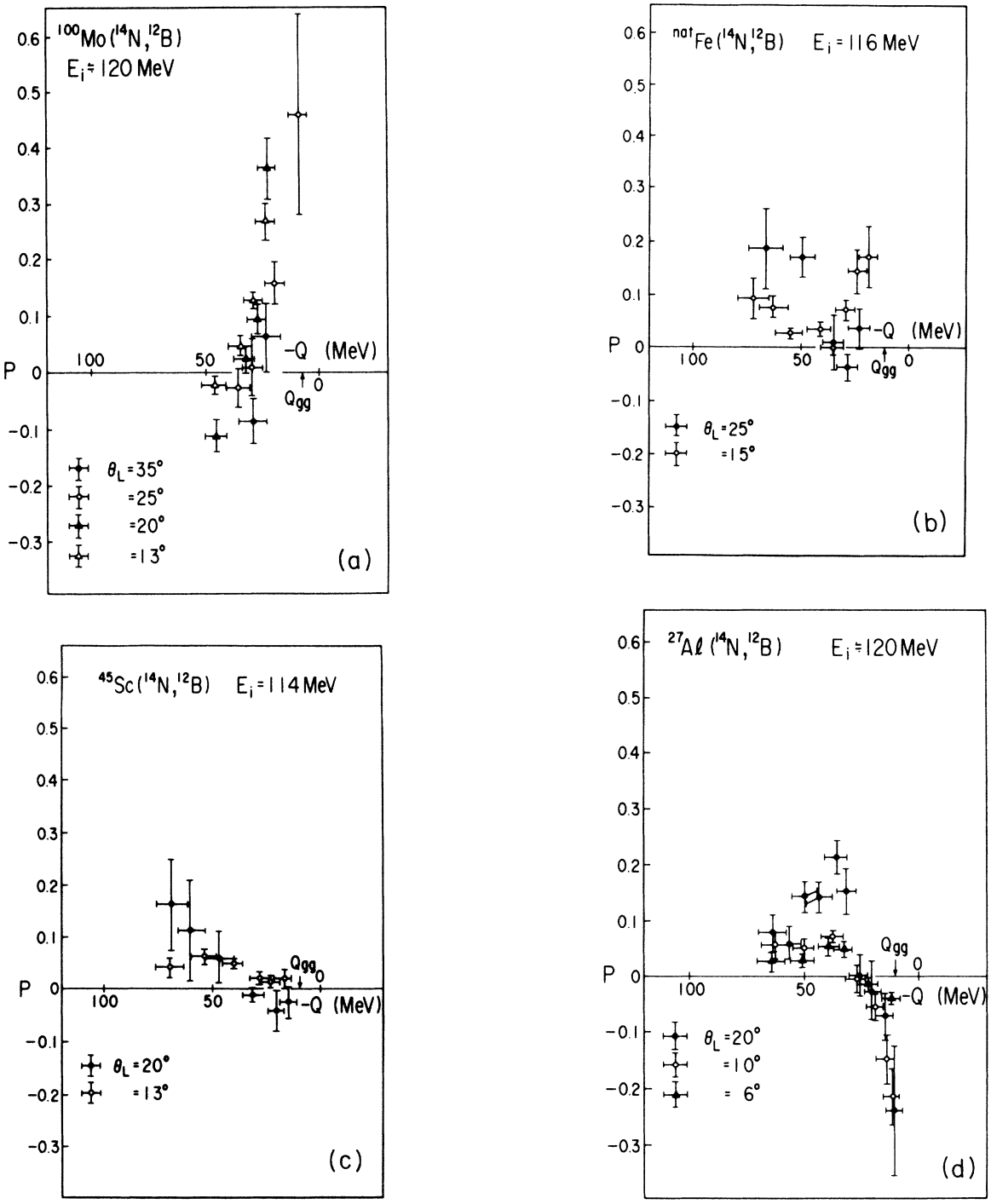


FIG. 11. (a)—(d) Superimposed illustration of the experimental polarization for various scattering angles.

ward angle.

The last feature, (5), may also be qualitatively understood in the framework of the classical friction model. Assuming the complete polarization of the reaction products from both positive- and negative-angle deflection processes, polarization is given by

$$P = -(\sigma_+ - \sigma_-)/(\sigma_+ + \sigma_-) . \quad (4.1)$$

Partial cross sections $\sigma_+$ and $\sigma_-$ in the positive- and negative-angle deflections, respectively, contribute destructively to polarization. Since the contribution from a positive-angle deflection becomes small at backward angles, polarization becomes large with its sign positive.

### A. Analysis in terms of the classical friction model

The gross properties of experimental $^{12}$B polarization have qualitatively been explained in the framework of the

classical friction model, except for the region of small energy loss with heavy target nuclei where the direct two-proton transfer process is dominant. In this section a quantitative analysis is given in the framework of the friction model of the systematic behavior of the experimental $^{12}B$ polarization.

Our concern here is the dependence of the second zero crossing (SZC) on the target mass number $A_2$, as discussed previously.[18] The reaction $Q$ values for the SZC observed near the grazing angle are shown in Fig. 12 as a function of $A_2$. The vertical bars show the uncertainty due to the width of the kinetic energy windows adopted in the experiment. The reaction $Q$ value for the SZC can be fitted with a straight line. Starting from this linear relation, the averaged friction constant $k$ is extracted for an interacting double-nuclear system (DNS) on the most probable trajectory. The formulae for the energy loss of the projectile-like fragment which comes from the far side of the target nucleus (negative-angle deflection) was extended to the present reaction, ($^{14}N$,$^{12}B$). Also, a microscopic treatment of heavy-ion reaction based on the quasi-linear response theory (QLRT) is applied to the ($^{14}N$,$^{12}B$) reaction.

First, the frictional force $\mathbf{f}$ is assumed to be proportional to the relative velocity $\mathbf{v}$ between the colliding nuclei, $\mathbf{f}=-k\mathbf{v}$, with the averaged friction constant[19] $k$. The kinetic energy loss $E_{\rm loss}$ resulting from the friction force is given as a function of the interaction time $\tau$ as

$$E_{\rm loss}=E_{\rm eff}[1-\exp(-2k\tau/\mu)] , \tag{4.2}$$

where $\mu$ is the reduced mass and $E_{\rm eff}$ is an effective incident energy[20] equivalent to the incident energy $E_{\rm c.m.}$ in the center-of-mass system measured from the top of the Coulomb barrier $V_{Ci}$ in the incoming channel. The interaction time $\tau$ is related to the rotation angle $\theta$ of the DNS and its angular velocity $\omega=J/I$, where $J$ and $I$ are the total angular momentum of the system and its moment of inertia, respectively. The moment of inertia $I$ of the DNS is written as $I=\mu R^2$, where $R$ is the distance between the centers of the projectile and target nuclei, and is the same as used in a proximity potential.[21] The orbital angular momentum $J$ brought into the DNS is $J=R(2\mu E_{\rm eff})^{1/2}$. For the $^{12}B$ ejected near the grazing angle, the rotation angle $\theta$ is roughly twice the grazing angle. Then,

$$\theta=2\theta_{\rm gr}=4\sin^{-1}[V_{Ci}/(2E_{\rm c.m.}-V_{Ci})] .$$

Since $E_{\rm c.m.}$ is much larger than $V_{Ci}$, the angle $\theta$ can be rewritten as $\theta=V_{Ci}/(2E_{\rm c.m.}-V_{Ci})$ by taking the leading term. Then the interaction time is written as

$$\tau=\theta/\omega=V_{Ci}R(2\mu/E_{\rm c.m.})^{1/2}/(E_{\rm c.m.}-V_{Ci}) . \tag{4.3}$$

Taking the leading term of Eq. (4.2) and approximating the atomic number $Z$ with $Z=A/2$, the energy loss resulting from the frictional force is expressed as

$$E_{\rm loss}=2k\tau(E_{\rm c.m.}-V_{Ci})/\mu$$
$$=k(A_1+A_2)(A_1/E_i)^{1/2}\times 10^{22}\ \text{MeV} . \tag{4.4}$$

Here, $A_1$ and $A_2$ indicate the projectile and target mass numbers, respectively. The solid line drawn in Fig. 12 is taken from Eq. (4.4) applied on the ($^{14}N$,$^{12}B$) reaction with a proper friction constant. The linear relation obtained in Eq. (4.4) suggests that $Q$(SZC) is a clear reference to $E_{\rm loss}$ on the most probable orbit of the reaction.

The averaged friction constant $k$ can be extracted from the following procedure in which the formalism is refined to include the information on reaction angle of the projectile-like fragment. The constant $k$ is calculated in the following expression derived from Eq. (4.2):

$$k=-(\mu/2\tau)\ln\left[\frac{E_{\rm c.m.}-V_{Cf}-E_{\rm loss}}{E_{\rm c.m.}-V_{Ci}}\right] . \tag{4.5}$$

Here, $V_{Cf}$ is Coulomb energy in the outgoing channel. The interaction time $\tau$ is determined from Eq. (4.3). However, the expression for the notation angle $\theta$ is modified in order to include the reaction angle as

$$\theta=\theta_{{\rm gr}i}/2+\theta_{{\rm gr}f}/2+\theta_{\rm c.m.} ,$$

where $\theta_{{\rm gr}i}$ and $\theta_{{\rm gr}f}$ are grazing angles for the incoming and the outgoing channels, as shown in Fig. 13, and $\theta_{\rm c.m.}$ is the reaction angle in the center-of-mass frame. Here, $\theta_{{\rm gr}i}=\theta_{\rm gr}$ and

$$\theta_{{\rm gr}f}=2\sin^{-1}[V_{Cf}/2(E_{\rm c.m.}-E_{\rm loss})-V_{Cf}] .$$

The $\theta_{\rm c.m.}$ is obtained from the reaction angle $\theta_L$ in the laboratory frame by using

$$\theta_{\rm c.m.}=\sin^{-1}(\eta\sin\theta_L)+\theta_L ,$$

where

$$\eta=\{168E_{\rm c.m.}/[A_2(A_2+2)(E_{\rm c.m.}-E_{\rm loss})]\}^{1/2}$$

for ($^{14}N$,$^{12}B$) reactions. The interaction time $\tau$ is then determined as the ratio of $J$ to $\theta I$.

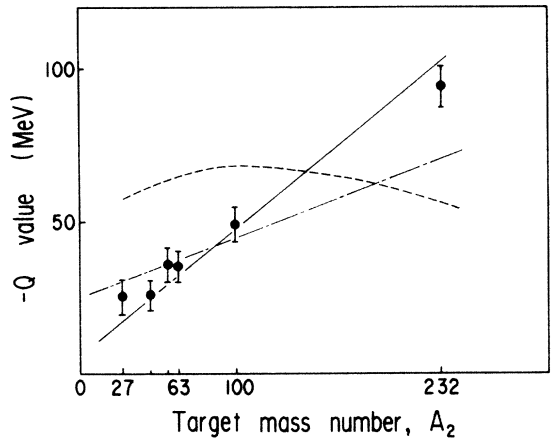


FIG. 12. Experimental $Q$ values of the SZC plotted against target mass number $A_2$. The vertical bars show the width of the kinetic energy ($Q$-value) window. The solid line is the most probable energy loss $E_{\rm loss}$ calculated from the friction model [Eq. (4.4), see text] with a friction constant $1.1\times10^{-22}$ MeV s/fm$^2$. $Q$ values for Coulomb energy at the final state of the collision (dashed line) under the assumption of spherical shape and $Q$ values of the SZC calculated by QLRT (dotted-dashed line) are also shown.

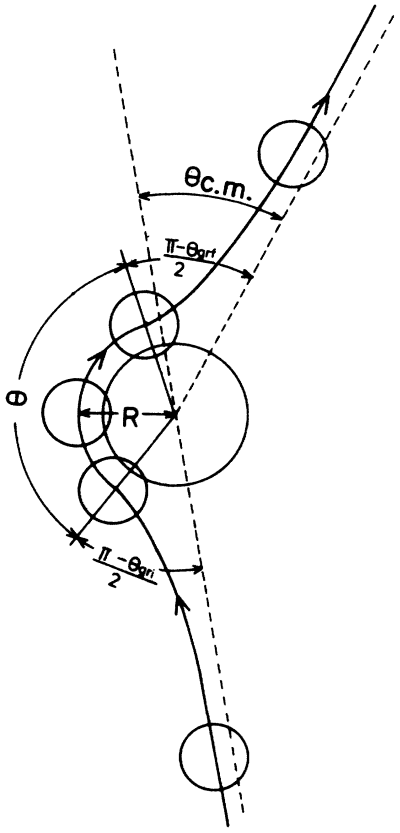


FIG. 13. Schematic illustration of a frictional scattering process used for the calculation of the friction constant.

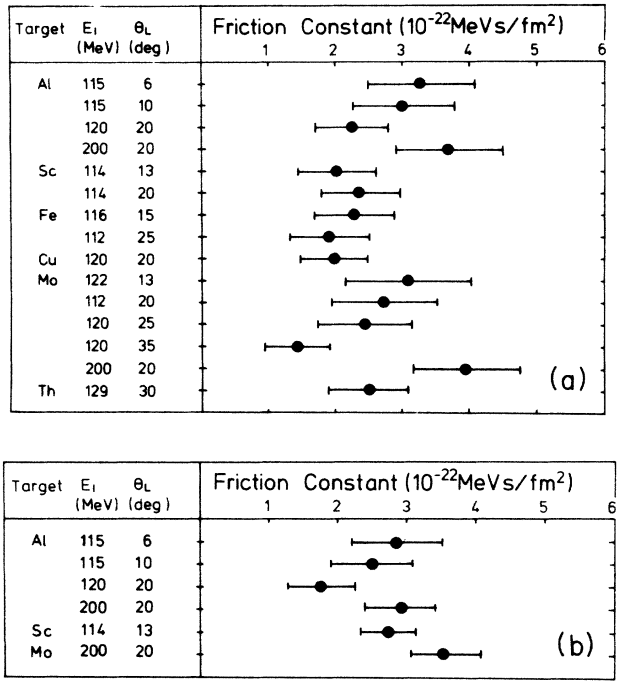


FIG. 14. Experimental results of the friction constant. The values used for $E_{\text{loss}}$ are (a) $-[Q(V_{Cf})+Q(\text{SZC})]/2$ and (b) $-Q$ for the largest positive polarization.

By solving the equation numerically, the friction constant $k$ is derived from the values of $E_{\text{loss}}$ related to the SZC. The SZC is the kinetic energy where the production yield from the far side of the target nucleus and that from the near side are of the same strength. If we consider the contribution solely of the negative-angle orbit, $E_{\text{loss}}$ is then expected to lie between $-Q(\text{SZC})$ and $-Q(V_{Cf})$, where $-Q(V_{Cf})$ is the $Q$ value corresponding to the Coulomb energy of two spherical nuclei in the final state of the collision. The dependence on $A_2$ of $-Q(\text{SZC})$ and $-Q(V_{Cf})$ is illustrated in Fig. 12. Except for target nucleus Th, $V_{Cf}$ is the least energy of an observed reaction product. The energy of the reaction product from Th($^{14}$N,$^{12}$B) is continuous not only to the $V_{Cf}$ calculated for two spherical nuclei but also extends below this energy. The effect of nuclear deformation is added in the calculation to modify the distance of the closest approach between the colliding nuclei, and the least kinetic energy observed for reaction product is considered to be $V_{Cf}$.

In this trial to extract the fraction constant $k$, $E_{\text{loss}}$ is chosen to be the mean values of $-Q(\text{SZC})$ and $-Q(V_{Cf})$. Errors in $E_{\text{loss}}$ are set to be one energy window at $-Q(\text{SZC})$. The results are in good agreement with each other, as shown in Fig. 14(a), and the averaged friction constant is $k=(2.4\pm0.5)\times10^{-22}$ MeV s/fm$^2$. The $-Q$ value for the largest positive polarization is supposed to be that for $^{12}$B in its most probable trajectory and is usually between $-Q(\text{SZC})$ and $-Q(V_{Cf})$. The friction constant deduced using this $Q$ value as $E_{\text{loss}}$ is very close to the previous values, as shown in Fig. 14(b). It should be noted that the $k$ value thus derived agrees in order of magnitude with that introduced by Schroeder *et al.*[20] Their value of the friction constant for the Xe + Bi reaction is $3\times10^{-22}$ MeV s/fm$^2$ and has been extracted by applying a transport model to the atomic number distribution of projectile-like fragments.

Although the calculation based on the assumptions described above gives us the reasonable friction constant, we improve the calculation based on a more realistic model. We include fluctuations of the trajectories around the mean classical orbit explicitly in the calculation when we regard the SZC as a reaction $Q$ value where the contributions from the far and near sides of the target nucleus are equal. Takigawa and co-workers have recently developed a new method of computation[22] in the framework of quasilinear response theory (QLRT) which is suitable for our purposes here. In this theory the energy transport from the relative motion to the intrinsic degree of freedom within nuclei is described by the Fokker-Planck equation. The calculated contour plots of the double differential cross section in the $E$-$\theta$ plane (Wilczynski plot) reproduces the experimental data well for the Ar + Th, Xe + Bi, and Pb + Pb systems.[23] In applying this theory to reactions between lighter ions, such as N + Al, however, the QLRT should be modified in order to include the mass transfer degree of freedom, which plays a kinematically important role in the reactions induced by ions of mass number $A_1<20$. For this purpose, the "projectile" is considered to have the mass number of the reaction product which has the same energy per nu-

cleon. The kinetic energy of the "projectile" is cut at the energy which corresponds to the $Q_{gg}$ value of the two-body transfer reaction in order to reject the elastic scattering. The parameters and formalisms are not changed in the present modification, except for the correlation length, a constant of 3.5 fm in the original QLRT which is replaced by a mass dependent form $0.65(A_1+A_2)^{1/3}$ fm. The results from the modified QLRT are compared with the experimental data on the double differential cross section for $^{14}$N-induced reactions,[24] and the reproduction of the fluctuation around the mean classical trajectory is good.

In this framework, the production cross sections $\sigma_+$ and the $\sigma_-$ in Eq. (4.1) are calculated as a function of reaction $Q$ value for various reaction angles and incident energies. Polarization is obtained according to Eq. (4.1) and is shown in Figs. 4, 8, and 10. The theoretical polarizations are multiplied by a factor 0.2. The theoretical polarization is in agreement with the measured one, except for that in the region of small energy loss for heavy target nuclei, and the SZC is also well reproduced as a function of $A_2$, as shown in Fig. 12. These facts mean that the main structure of the $^{12}$B polarization reflects the contribution of frictional processes in heavy-ion reactions. The experimental value is still one-half of the calculated. It should be noted that the polarization diluted by the various processes diminishes the amount to 40%, as estimated in Sec. III C. This fact suggests that the assumption of the complete polarization in the reaction products in the frictional process is not correct and/or some depolarization mechanism should be introduced in the collision model. Reif and co-workers have also applied a friction model to $^{14}$N-induced reactions including statistical fluctuations[25] and their deflection functions qualitatively reproduce the present experimental results.

### B. Coexistence of the two different reaction mechanisms

The variation of the first zero crossing (FZC) with the target mass number $A_2$ and the measurement angle $\theta_L$ in the region of small kinetic energy loss is understood by assuming the coexistence of the two different reaction mechanisms. From the sign of polarization measured near $Q_{gg}$ for various $A_2$, the frictional process is disclosed to be a dominant mechanism for light target nuclei, such as $^{27}$Al, and is found to be competing equally with the direct process for target nuclei $^{45}$Sc. From our previous work,[2,3] the main process of $^{100}$Mo($^{14}$N,$^{12}$B) near $Q_{gg}$ is known to be the direct process. A small contribution from a frictional process, however, mixes with it, and the negative polarization from the frictional process is superimposed on the polarization from the direct process.

The ratio of the contributions from the two processes can be estimated, provided the negative polarization resulting from the frictional process is $P_0$ independently of $Q$ value, and the polarization from the direct process decreases linearly with $Q$ value, the slope of which is $\zeta=\Delta P/\Delta Q=-0.02$. The $Q$ value of the FZC, $Q_1$, is then given by

$$Q_1=Q_0+P_0a/[(1-a)\zeta]\,, \tag{4.6}$$

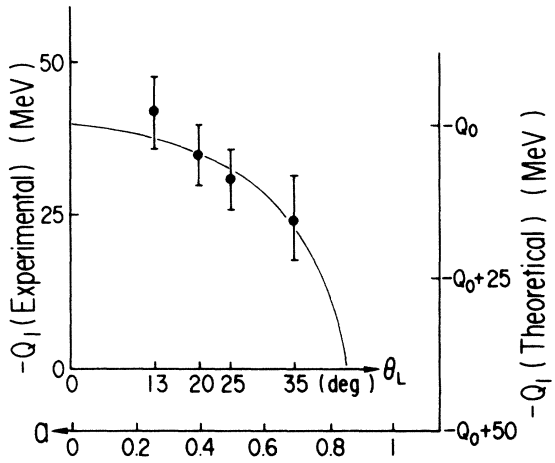


FIG. 15. Experimental $Q$ values corresponding to the FZC plotted against the scattering angle for $^{100}$Mo($^{14}$N,$^{12}$B). The curve is calculated under the assumption of coexistence of frictional and direct processes. The vertical bars indicate the width of the kinetic energy window.

where $Q_0$ is the $Q$ value of the FZC for the pure direct process and $a$ is the fraction of the frictional process $(0\le a\le 1)$. Equation (4.6) is fitted to experimental $Q$(FZC) for $^{100}$Mo as a function of the reaction angle $\theta_L$, as shown in Fig. 15, assuming that $a$ is proportional to $\theta_L$. The value of $P_0$ is chosen as 0.15, as observed near $Q_{gg}$ for the target nucleus $^{27}$Al at the grazing angle. From this fitting, it is deduced that the fraction $a$ increases to approximately 70% at the reaction angle $\theta_L=35°$.

### C. Comparison with the other experiments

Polarization of the first excited state of projectile-like fragment in the reactions Ni($^{16}$O,$^{16}$O) and Ni($^{16}$O,$^{12}$C) has been studied at an incident energy of about 100 MeV from the measurement of the circular polarization[5,26] of the emitted $\gamma$ ray. The discrete $\gamma$ rays were separated from the continuum by use of particle-$\gamma$ coincidence technique.

In the alpha transfer reaction Ni($^{16}$O,$^{12}$C), dependence of polarization on the reaction $Q$ value obtained by Trautmann *et al.* is similar to our result for $^{nat}$Cu($^{14}$N,$^{12}$B) [see Fig. 4(c)]. In the region of small energy loss, the positive polarization which corresponds to the direct cluster transfer is observed. The sign of the polarization becomes negative with increasing kinetic energy loss and returns to a positive value for large energy loss. This behavior of the polarization is typical for the frictional process. In the inelastic channel, polarization is similar to our results on $^{27}$Al($^{14}$N,$^{12}$B) [see Fig. 4(f)]. The characteristic positive polarization from the direct cluster transfer is completely suppressed and the trend of the polarization can be explained solely by the frictional process. These facts clearly indicate the contribution of the frictional process in heavy-ion reactions. Also indicated is the direct transfer process competing with the frictional one in the region of small energy loss. Thus it can be concluded that the polarization measured via the $\gamma$-ray method qualitatively agrees with our systematic measurement.

## V. CONCLUSIONS

Polarization of $^{12}$B produced in ($^{14}$N,$^{12}$B) reactions has been measured around grazing angles at two incident energies. The systematic behavior of polarization has been observed and understood within the framework of the classical friction model. This model, with the concept of a classical trajectory, explains satisfactorily the behavior of polarization. Thus it is concluded that an approximate description of heavy-ion reactions in terms of a classical picture has been accomplished. The friction constant has been deduced from the present experimental data to be $(2.4\pm0.5)\times10^{-22}$ MeV s/fm$^2$.

Polarization observed in the region of small energy loss for the reactions with targets heavier than $^{nat}$Fe is interpreted in terms of the direct two-proton transfer process from the projectile to the target nuclei. This process is, however, strongly suppressed in light target nuclei; here, the main feature of polarization is explained exclusively by the frictional model. This behavior of polarization indicates that the two processes, frictional and direct, compete in the region of small energy loss. This is possible because the interaction time and the energy loss in the frictional process are smaller for lighter target nuclei than those for heavier target nuclei. The sign of the polarization in the region of small energy loss is determined by a balance between two contributions from the direct process and the frictional process.

## ACKNOWLEDGMENTS

We would like to express our thanks to Professor K. Sugimoto and Dr. Y. Miake for their contribution throughout the present study. Professor N. Takigawa and Dr. K. Niita kindly permitted us to use their computer program "Quasi-Linear Response Theory" for the analysis of the experimental results. Mr. Y. Takahashi and Mr. M. Sakamoto provided technical assistance. All the experiments described here were carried out at the Research Center for Nuclear Physics (RCNP), Osaka University, under the program numbers 4A-15, 5A-17, 6A-18, 7A-19, 8A-22, 9A-17, 10A-02, 11A-20, 12A-20, 13A-12, and 14A-19. The staff and cyclotron crew of RCNP are highly appreciated for their cooperation. The present study was supported in part by the Grant-in-Aid of Scientific Research, Ministry of Education, and by Toray Science and Technology Grants.

---

*Present address: National Laboratory for High Energy Physics, Oho-Machi, Tsukuba-Gun, Ibaraki-Ken, 305 Japan.

†Present address: Institute for Physical and Chemical Research, Wako-Shi, Saitama, 351 Japan.

‡Also at College of General Education, Osaka University, Toyonaka, Osaka, 560 Japan.

[1]J. Wilczynski, Phys. Lett. **47B**, 484 (1973).

[2]K. Sugimoto *et al.*, Phys. Rev. Lett. **39**, 329 (1977).

[3]N. Takahashi *et al.*, Phys. Lett. **73B**, 281 (1978).

[4]W. Trautmann *et al.*, Phys. Rev. Lett. **39**, 1062 (1977) and W. Trautmann *et al.*, Nucl. Phys. **A422**, 418 (1984).

[5]W. Trautmann *et al.*, Phys. Rev. Lett. **46**, 1188 (1981).

[6]M. Ishihara *et al.*, Phys. Lett. **73B**, 281 (1978).

[7]A. G. Artukh *et al.*, Nucl. Phys. **A160**, 511 (1971).

[8]K. Asahi *et al.*, Nucl. Instrum. Methods **220**, 389 (1984).

[9]L. C. Northcliffe and R. F. Schilling, Nucl. Data Tables A **7**, 233 (1970).

[10]T. Minamisono, J. Phys. Soc. Jpn. Suppl. **34**, 324 (1973).

[11]J. C. Wells, Jr., R. L. Williams, Jr., L. Pfeiffer, and L. Madansky, Phys. Lett. **27B**, 448 (1968).

[12]K. Sugimoto, K. Nakai, K. Matsuda, and T. Minamisono, J. Phys. Soc. Jpn. **25**, 1258 (1968).

[13]M. Morita, *Beta Decay and Muon Capture* (Benjamin, New York, 1973), p. 64.

[14]N. Takahashi *et al.*, in *Polarization Phenomena in Nuclear Physics—1980 (Fifth International Symposium, Sante Fe)*, Proceedings of the Fifth International Symposium, AIP Conf. Proc. No. 69, edited by G. G. Ohlson, R. E. Brown, N. Jarmie, W. W. McNaughton, and G. M. Hale (AIP, New York, 1981), p. 1114; N. Takahashi, *ibid.*, p. 1016; T. Minamisono *et al.*, Hyperfine Interact. **9**, 53 (1981).

[15]R. Ost *et al.*, Nucl. Phys. **A265**, 142 (1976).

[16]J. W. Olness and E. K. Warburton, Phys. Rev. **166**, 1004 (1968); L. F. Chase, Jr., R. E. McDonald, W. W. True, and E. K. Warburton, Phys. Rev. **166**, 997 (1968).

[17]A. G. Artukh *et al.*, Nucl. Phys. **A215**, 91 (1973).

[18]K. H. Tanaka, Ph.D. dissertation, Osaka University, 1983; T. Minamisono *et al.*, Hyperfine Interact. **15/16**, 25 (1983).

[19]R. Beck and D. H. E. Gross, Phys. Lett. **47B**, 143 (1973).

[20]W. U. Schroeder *et al.*, Phys. Rep. **45**, 301 (1978).

[21]J. Blocki, J. Randrup, W. J. Swiatecki, and C. F. Tsang, Ann. Phys. (N.Y.) **105**, 427 (1977).

[22]N. Takigawa, K. Niita, Y. Okuhara, and S. Yoshida, Nucl. Phys. **A371**, 130 (1981).

[23]K. Niita and N. Takigawa, Nucl. Phys. **A397**, 141 (1983).

[24]T. Fukuda *et al.*, Phys. Lett. **99B**, 317 (1981).

[25]R. Schmidt and R. Reif, J. Phys. G **7**, 775 (1981); R. Reif and G. Saupe, *ibid.* **8**, L21 (1982).

[26]W. Dunnweber, J. Phys. Soc. Jpn. Suppl. **55**, 234 (1986).